The impact of ambient pressure and tunnel inclination angle on the smoke transport in a subway tunnel

Guang Chen (gszxcgsq@163.com)
Central South University

Research Article

Keywords: Subway fire, Tunnel inclination, Overset mesh, Ambient pressure, Piston wind

Posted Date: July 22nd, 2021

DOI: https://doi.org/10.21203/rs.3.rs-738218/v1

The impact of ambient pressure and tunnel inclination angle on the smoke transport in a subway tunnel

Xi-Feng Liang [a, b, c], Guang Chen [a, b, c*], Xiao-Bai Li [a, b, c], Zhen Liu [d]

[a] Key Laboratory of Traffic Safety on Track (Central South University), Ministry of Education, Changsha, 410000, China

[b] Joint International Research Laboratory of Key Technology for Rail Traffic Safety, Changsha, 410000, China

[c] National & Local Joint Engineering Research Centre of Safety Technology for Rail Vehicle, Changsha, 410000, China

[d] School of Civil Engineering, University of Birmingham, Birmingham, UK

***Corresponding author**

Tel.: +86+15243643542

Email address: gszxcgsq@163.com

ABSTRACT: The subway tunnel will be built in the plateau where the pressure is relatively low, and the tunnel will tilt at a certain angle due to topographic factors. In order to investigate the smoke transport characteristics of moving subway trains caught fire under different ambient pressures and different tunnel inclination angles, three-dimensional full-scale calculation models of subway trains, two stations and one tunnel are established, and three different environmental pressures (50kPa, 75kPa, 100kPa) and three different tunnel inclination angles (- 1.5 °, 0 °, + 1.5 °) are simulated. The IDDES turbulence model based on kω-sst RANS combined with the overset grid technology is used to simulate the subway train movement and the detailed flow field. The velocity and temperature distribution characteristics and smoke concentration field are studied in detail. The soot density of smoke and temperature increases with reduced ambient pressure due to the weakening of air entrainment and the decreased air density and the influence of ambient pressure on smoke diffusion decreases with the increase of pressure. The longitudinal airflow induced by the stack effect under the negative inclination angle of the tunnel is helpful to prevent the flowing back of smoke.

Keywords: Subway fire; Tunnel inclination; Overset mesh; Ambient pressure; Piston wind;

1 Introduction

With the continuous development of social economy, subway traffic has gradually become an indispensable part of urban traffic structure due to its characteristics of fast, large traffic volume, small pollution, and high efficiency. According to statistics, by the end of December 2019, there were 38 cities in China that had opened metro, with a total operating mileage of 5,480 kilometers(Liu and Li, 2020). Although the construction of subway line greatly alleviates the pressure of urban ground transportation and brings convenience to residents' life, the frequent operation of subway also brings a lot of safety problems. Fire, as the main form of disaster, attracts people's extensive attention. Due to the complex structure of subway system, the occurrence, development and development of fire have particularity. Once a fire occurs, the fire situation is complex, which can easily cause huge casualties and property losses. In the process of continuous operation, the heat and smoke generated by the fire accumulate and spread rapidly in the subway tunnel. The operation of the train makes the propagation behavior of fire smoke in the tunnel more complex (Wang et al., 2020; N. Zhang et al., 2018a). So, it is urgent to carry out the research on the operation of train carrying fire sources and the law of fire smoke transport in subway tunnels and stations.

Subway is an underground enclosed building, and the occurrence of subway fire is the most harmful one in subway accidents, which can easily cause mass death and mass injury of people, and it is difficult to evacuate and rescue. Therefore, countries all over the world have

invested plenty of manpower and material resources to conduct extensive research on the characteristics of subway fire smoke under the effect of various factors, mainly using the three methods of full-size fire test (Cafaro and Bertola, 2014; Hu et al., 2005; Lemaire and Kenyon, 2006; Tian et al., 2017; Wang et al., 2009; Weng et al., 2014; Yan et al., 2009), fire model test (Chaabat et al., 2020; Chow et al., 2017, 2011; Ji et al., 2016; Oka and Atkinson, 1995; Tang et al., 2017; Vauquelin and Mégret, 2002; Vauquelin and Telle, 2005; Zhang et al., 2017, 2016) and numerical simulation (Bai et al., 2016; Gannouni and Maad, 2015; Hu et al., 2013b; Ji et al., 2013; Ko and Hadjisophocleous, 2013; Lee and Ryou, 2006; Tang et al., 2017; Wang et al., 2020; N. Zhang et al., 2018a). With the continuous maturity of test conditions, test equipment and test technology, the development scope of full-size tunnel fire test is further expanded, the test content is constantly expanded, and the accumulated test data is more comprehensive, which provides a lot of valuable experience for the development of tunnel engineering. However, due to the high cost of individual test, less measurable content, low repeatability and other factors, it is not easy to conduct a comprehensive study of tunnel fire.

Therefore, research methods such as model test and numerical simulation method are gradually derived. Compared with model test research, numerical calculation has the advantages of low cost, fast calculation speed and comprehensive output results, and can calculate all parameters in the whole calculation area. Therefore, many scholars use numerical simulation methods to simulate subway fire research. However, at present, scholars at home and abroad are studying and analyzing the static fire source utilization model test and CFD. Their work mainly focuses on four aspects: (1) the back-layering length and critical velocity under different heat release fire(Du et al., 2020; Meng et al., 2018; Tang et al., 2016; Wang et al., 2016; Weng et al., 2016; Y. Yao et al., 2016).(2) the distribution of smoke and temperature field inside the tunnel(Hu et al., 2013a, 2013b; Ji et al., 2019; Li et al., 2011; Meng et al., 2017; Tian et al., 2017).(3) the smoke extraction efficiency using combined natural and forced ventilation(Cong et al., 2017; Fan et al., 2017; Jiang et al., 2018; Mei et al., 2017; Z. Zhang et al., 2018).

However, in the case of moving subway train on fire, the research on smoke transport and temperature distribution is relatively few. The fire characteristics of moving trains will be seriously affected by the piston wind induced by the train movement. X. Zhang et al. (2019) carried out numerical simulation with IDA Tunnel software, studied the four parameters of open and closed system, by-pass ducts, train intervals and adjustable vent, and analyzed the air inflow rate at the gate of the adjustable station. Zhong et al. (2015) numerically studied the smoke transport of subway fire under the effect of piston wind and put forward three methods to reduce

the effect of the piston wind on smoke layer transport. The detailed analysis of the flow field, temperature field and velocity distribution shows that the piston wind produces a large range of eddy current and horizontal inertia force, which destroys the stratification of smoke layer. Xie et al.(2010) investigated the smoke transport of the moving train on fire using CFD and the research shows that the train piston wind plays a leading role in the transport of the smoke, and the flowing back phenomenon of the smoke almost does not exist. In the process of continuous operation and evacuation, the upstream compartment is basically unaffected, and the temperature and smoke concentration in the downstream compartment increase with time, and tend to be stable when the fire reaches the maximum scale. D. Zhou et al. (2015) used dynamic grid technology to study the distribution of smoke field in the tunnel when the subway head train catches fire at the bottom of the train. The results present the piston wind induced by train movement plays a decisive role in the transport of smoke in the tunnel. The direction of mechanical ventilation should be consistent with the running direction of the train to prevent smoke from continuing to spread upstream in the tunnel. N. Zhang et al.(2018) established a three-dimensional full-scale model and used the dynamic grid technology to study the effect of the blockage ratio and train speed on the transport of smoke and temperature distribution in the tunnel when the subway train caught fire. The smoke movement is basically the same as that of D. Zhou et al. (2015). when the train is running normally and decelerating, the smoke moves to the tail (upstream). The slipstream formed during the train moving plays a leading role in the smoke movement in the tunnel, which makes the smoke flow to the front region of the train (downstream). After the slipstream weakens until it disappears, the smoke will spread to the tail (upstream) again. In this paper, it is pointed out that the effect of block ratio on smoke movement is more significant than the speed of train.

At present, the research on the smoke transport of moving train on fire under different ambient pressure and tunnel inclination angle is not deep enough. The effects of ambient pressure and tunnel inclination on the smoke movement and temperature distribution of the static fire in tunnel have been studied by Jie Ji et al. (2017, 2019). In order to study the influence of train movement on the transport characteristics of smoke under different ambient pressure and tunnel inclination in detail, this paper establishes a model involving a 3-D full-scale subway train and the IDDES turbulence model based on kω-sst RANS combined with the overset grid technology is used to simulate the subway train movement and the detailed flow field.

2 Numerical methods

2.1 Geometry model

To realistically simulate the blockage effect of a vehicle and realistically describe the smoke flow characteristics, a 1:1 3D subway train consisting of 6 cars is used in this study, as shown in Fig.1. The model train has a length of 140m $(25\times2+22.5\times4)$, and the cross-sectional area of the subway train body is 9.5m^2. Certain components, e.g., the bogie, apron, head, windshield, and equipment cabin, which have a strong influence on the flow of smoke, are modeled in detail. According to incomplete statistics of subway fire accidents(H. W. Yao et al., 2016), approximately 46% of subway train fire accidents are due to equipment failure, such as electrical equipment and brakes, which are mostly located at the bottom of the train. As the fire source moves with the train, the smoke has the greatest influence on the rear carriages when the fire occurs in the first carriage. Therefore, the location of the fire source is set at the bottom of car 1, the dimension of the fire is 8m×2m×1m [3], as shown in Fig. 1. The profile and basic dimensions of the tunnel section used in the numerical simulation in this paper are shown in Fig. 2, and the cross-sectional area of the tunnel is 25m^2, so the blocking ratio ($BR = A_{train}/A_{tunnel}$) is 0.38.

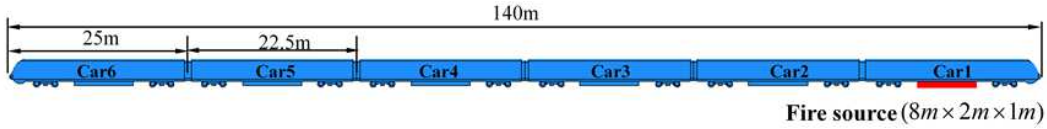

Fig. 1. The subway train model used in numerical simulation.

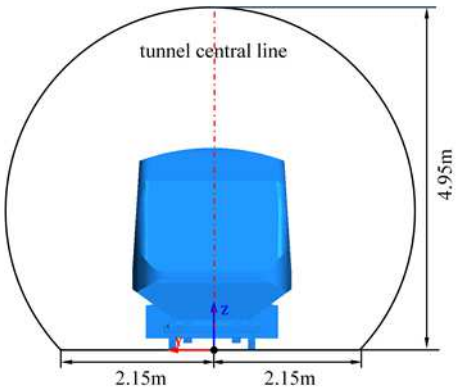

Fig. 2. The tunnel model used in numerical simulation.

2.2 Computational domain and boundary conditions

The physical model used in this paper consists of a 6-car subway train and two stations connected by a 1500 m long tunnel, as shown in Fig. 3. Each station has dimensions of

$100m \times 20m \times 10m$. The train is forced to stop in the center of the tunnel ($x = 750m$) due to the fire effect. The initial position of the train is at $x = 350m$, and the train runs for 10s at the speed of $20\,m/s$ ($72\,km/h$). When a fire breaks out, the train decelerates at an acceleration of $-1\,m/s^2$, and when it decelerates to 0, the train stops at the position of $x = 750m$, as shown in Fig. 3. The fire lasts 240s, corresponding to the time required to wait for rescue after stopping. Fig. 3 also shows the definition of the coordinate system (x, y, z). The center of the track was $y = 0$ (lateral direction), and the ground of the tunnel was $z = 0$ (vertical direction) and the entrance of the tunnel was $x = 0$ (longitudinal direction). According to the TSI regulation, the ground clearance was set to 0.235 m at full scale. The boundary conditions were specified as follows: a pressure outlet for the outlet, non-slip wall condition for the train body and tunnel wall. The numerical simulation was performed on the scale of 1:1. In addition, the maximum running velocity of the train was $20\,m/s$, corresponding to a Reynolds number of 4×10^6 .

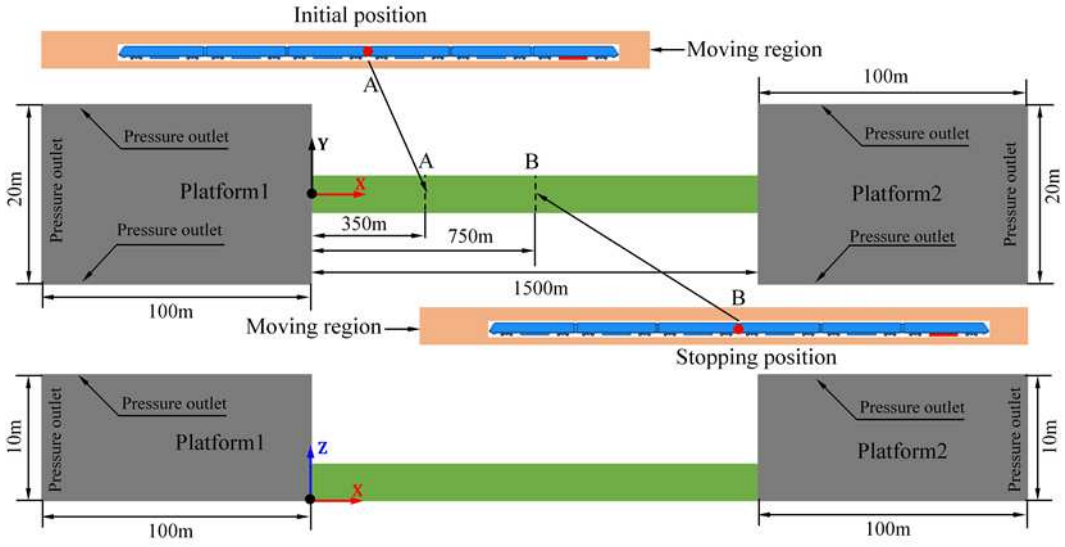

Fig. 3. Computational domain. (a) Top view, (b) Front view

2.3 Meshing strategy

In this paper, it is necessary to carefully simulate the influence of slipstream on smoke transport caused by train movement. according to previous articles on slipstream(Chen et al., 2019; Li et al., 2019; Liang et al., 2020), so the IDDES turbulence model based on the $k-\omega$ turbulence model is adopted in this paper. Mixed grids were used in the entire computation domain, which contained prism layers at the wall boundaries (train surface and tunnel wall) and hexahedral grids in the stationary region (SR) and polyhedral mesh in the moving region (MR), as shown in Fig. 4. Considering the effect of boundary layers on the surfaces of the tunnel and train body, the 16 prism grids with a growth rate of 1.1 around the tunnel wall and train body are generalized to resolve the near-wall flow structure. The thickness of the first boundary layer

was approximately 2 mm, to ensure that the averaged Y+ was approximately 2, which met the demands of the $k-\omega$ turbulence model. To verify the grid independence, three different mesh numbers were compared. the details of the differences between the four grids are listed in Table 1. Three sets of grids, i.e., coarse, medium, and fine grids, containing 17.6 million cells, 27 million cells, and 38.7 million cells, respectively, were used to test the grid sensitivity of the simulation. The medium grid distribution around the train is shown in Fig. 4.

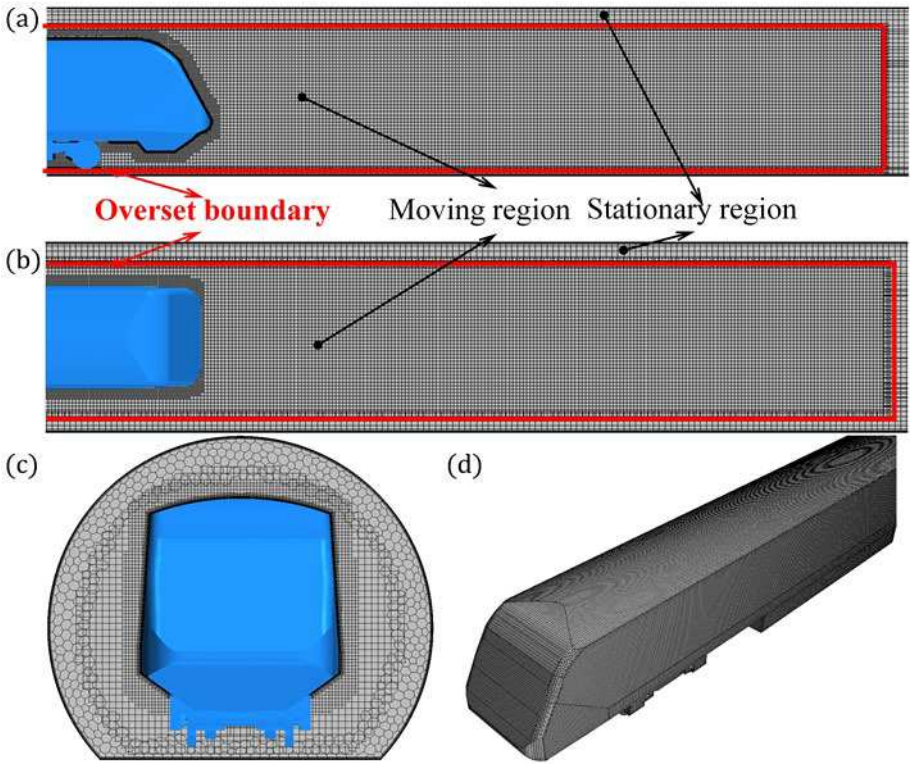

Fig. 4. Medium grid distribution around the train. (a) train surface, (b) bogie surface, (c) station surface.

Table 1. Spatial resolutions for three types of grids

Grid Density	Surface grid(m)		ΔL_x (m)	MR	SR	Total grid/$\times 10^5$
	Train surface	Tunnel surface				
Fine	0.05	0.15	0.15	177	210	387
Middle	0.06	0.20	0.20	120	150	270
Coarse	0.075	0.25	0.25	76	100	176

2.4 Fire source model

It is difficult to provide a model to describe the fire development process due to the complex combustion process, so the subway fire source is simplified to a fixed heat release rate (HRR) model. The most used unsteady HRR model is the t^2-model applied in Star-CCM+ software. According to the user guide, there are four types of t^2-model: slow, medium, fast,

and ultra-fast, the corresponding fire growth factor, respectively 0.0029, 0.01127, 0.04689, 0.1876.

$$Q = \alpha t^2 \tag{1}$$

where α is the fire growth factor. Taking the fast model as an example, the HRR requires nearly 3min to reach a maximum of 10MW, so we artificially crank up the value of α to 500000 in order to make the fire quickly reach a stable state and study the distribution of smoke and temperature in the tunnel when the fire source is stable. The fire size is set to 8m × 2m × 1m, and the fire heat release rate is 10MW according to the European UPTUN tunnel project (Migoya et al., 2011; N. Zhang et al., 2018b). The amount of soot released by burning one gram of fuel is 0.118 g. The smoke release rate is set according to the principle of oxygen consumption: $1.69\times10^4 KJ$ of heat is released per kilogram of oxygen consumed. To simulate the smoke particles, it is necessary to set the smoke yield in the VHS model. The smoke yield can be calculated according to the heat release rate, as follows:

$$Y_s = Y_{sm}\frac{Q}{H} \tag{2}$$

Where Y_s is the smoke yield, Y_{sm} is the smoke yield per unit mass ($0.118\ g/g$), H is the combustion heat ($16900\ kJ/kg$)(Zhou et al., 2020)(Overview and Guide, n.d.).

2.5. Radiation model

Radiative heat transfer is energy transferred through electromagnetic waves. The black body intensity is expressed as:

$$E_{b\lambda} = \frac{2\pi hc_0^2}{\lambda^5[e^{hc_0/\lambda k_B T}-1]} = \frac{2C_1}{\lambda^5(e^{C_2/\lambda T}-1)} \tag{3}$$

Where h is Planck's constant, c_0 is speed of light, λ is the wavelength inside the medium, k_B is the Boltzmann's constant, $C_1 = 0.6\times10^{-16} Wm^2/s$ and $C_2 = 0.01439 mk$.

When the radiation passes through the simulation region, the transfer equation (RTE) controls the change of the radiation intensity I in the direction of Ω. This equation can be written in terms of radiant intensity for a specific wavelength λ:

$$\frac{dI_\lambda}{ds} = k_{a\lambda}I_{b\lambda} - (k_{a\lambda}+k_{s\lambda})I_\lambda \tag{4}$$

Where I_λ is the radiative intensity at wavelength λ, $I_{b\lambda}$ is the black body intensity at wavelength λ, $k_{a\lambda}$ is the absorption coefficient at wavelength λ, $k_{s\lambda}$ is the scattering coefficient at wavelength λ and s is the distance in the Ω direction. The first term is the gained intensity for the heat emission and the second term is the lost intensity due to the absorption and scattering effect.

Discrete Ordinate Method (DOM) in STAR CCM+ is used in this paper to simulate the radiation effect. The DOM is a numerical model for describing radiative heat transfer in a simulation region. Within the DOM module, the gray thermal radiation model makes it possible to simulate diffuse radiation independently of wavelength. In this model, the radiation characteristics of the region and the surface are the same for all wavelengths. The surface radiative properties are quantified in terms of emissivity, specular and diffuse reflectivity, transmissivity, and radiation temperature. And the Kirchhoff's law is used to enforce the sum of the emissivity, reflectivity, and transmissivity to be 1.0 at surfaces. The discrete ordinates method participating media radiation solver in the STAR-CCM+ code is used to compute the radiative heat flux to the tunnel region in the three cases. The ordinate set of S8 is used for the discretization of DOM to ensure the balance between accuracy and computing time. This is 80 ordinates computed as $Sk = k(k+2)$. equations to cover all solid angles.

2.6 Numerical method

The simulations that are presented in this article were made using a segregated compressible finite-volume solver STAR-CCM+13.04. The fire-smoke flow control equations used in this paper are based on 3-D, compressible, unsteady Navier–Stokes equations. And the IDDES turbulence model based on the $k-\omega$ turbulence model combined with overset grid method were used to model the movement of the subway train and the detailed flow field inside the tunnel. To discretize the convective terms, a hybrid numerical scheme was used Moreover, a second-order upwind scheme was used for the turbulent quantities, while a second-order implicit scheme was used for the time integration. The discretized time step was $0.025\,t^*$ (where t^* is the non-dimensional time equal to H/U_{train}, H is the train height) before the subway train stops and the time step was increased to $0.25\,t^*$ after the train stops.

The equations are closed by regarding the air as a perfect gas satisfying the state equation:

$$P = \rho RT \tag{5}$$

where P is the pressure, R is the gas constant, and T is the temperature.

3 Numerical validation

3.1. Validation of the CFD method (Stationary fire in tunnel)

The static fire in the tunnel has been widely studied and there are a series of detailed experimental and numerical simulation data. In this section, the published temperature distribution in the tunnel is used to verify the calculation model, to accurately simulate the smoke transport process. It is verified that the model tunnel is a typical highway tunnel, the fire

size is $150m \times 10m \times 5m$ and the fire source is located in the center of the width of the tunnel, the distance from the left opening is 50m, the initial ambient temperature is $20^{\circ}C$, and the temperature measuring position is shown in Fig. 5. The ratio of characteristic fire diameter to grid size $D^*/\delta x$ is recommended in the range of 4-16, which has been widely used to evaluate grid resolution. D^* is expressed as:

$$D^* = \left(\frac{\dot{Q}}{\rho_0 c_p T_0 \sqrt{g}} \right)^{2/5} \tag{6}$$

Where $\dot{Q}$ is the heat release rate, ρ_0 is the air density, c_p is the specific heat capacity and T_0 is the ambient temperature. The fire heat release rate (HRR) is 10MW and the ambient pressure is 50 kPa, the characteristic fire diameter is 3.2 m, the recommended grid size range is about 0.2–0.8 m, so the 0.2m grid size is chosen for the simulation. Fig. 6 (a) shows longitude temperature distribution 0.1 m beneath the top tunnel surface. The temperature distribution of RANS model and IDDES model are basically consistent with those of Ji et al.[46] (FDS). It is worth noting that the IDDES model result is the average temperature field, the fluctuation characteristics of the temperature field of the IDDES model can be seen in Fig. 6 (b) which shows the variation curve of temperature with time at different longitudinal distances from the downstream of the fire source and Fig. 7 which shows the temperature field near the fire source. The IDDES model can better capture the dynamic characteristics of smoke transport, so this paper uses IDDES model for the simulation of moving train on fire.

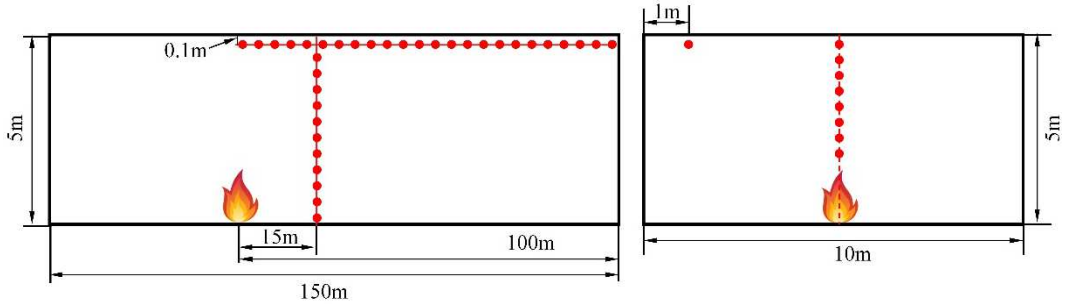

Fig. 5. Medium grid distribution around the train. (a) train surface, (b) bogie surface, (c) station surface.

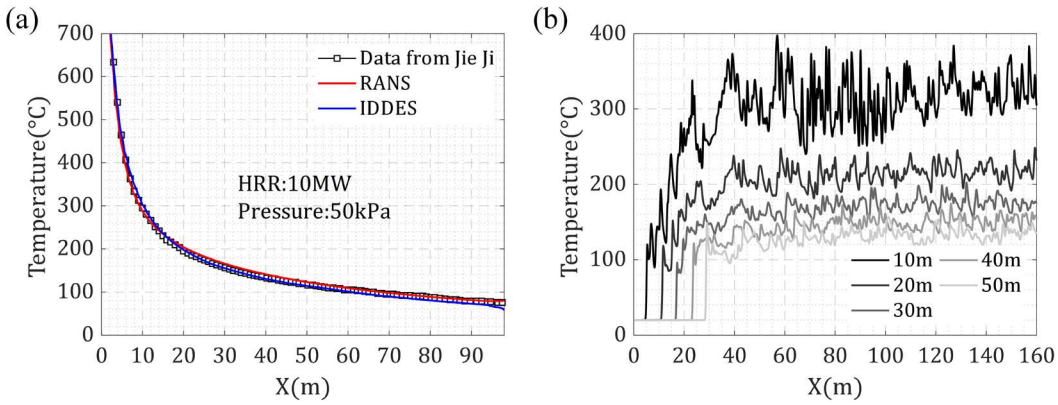

Fig. 6. (a) Longitude temperature distribution 0.1 m beneath the top tunnel surface. (b) Temperature at the point 0.1m below tunnel ceiling at different longitudinal distance downstream the fire source with time.

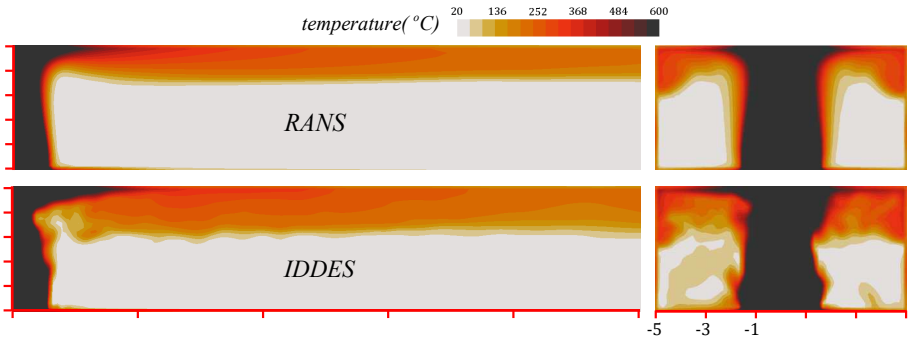

Fig. 7. Temperature field near the fire source.

3.2. Validation of the CFD method (Grid independence)

Grid refinement can affect the CFD prediction. In this paper, three different meshes of coarse mesh, medium mesh and fine mesh are studied to eliminate the influence of grid size and distribution. The three grids adopt the same scale partition strategies, using the same thickness and layer number of surface layer to maintain the same Y+ and only changing the distribution of train and tunnel surface. The three types of grids are about 17.6million, 27 million and 38.7 million respectively. Fig. 8 (a) shows that the longitude temperature distribution 0.2 m beneath the top tunnel surface under 70kPa ambient pressure at 240 s and Fig. 8 (b) is its local magnification. It can be seen from Fig. 8 that the temperature curves of the three mesh densities do not differ much, and the variation laws are basically the same. The maximum temperature under coarse mesh is slightly larger than that of middle meshes and fine meshes. In this paper, medium grid is used for numerical simulation.

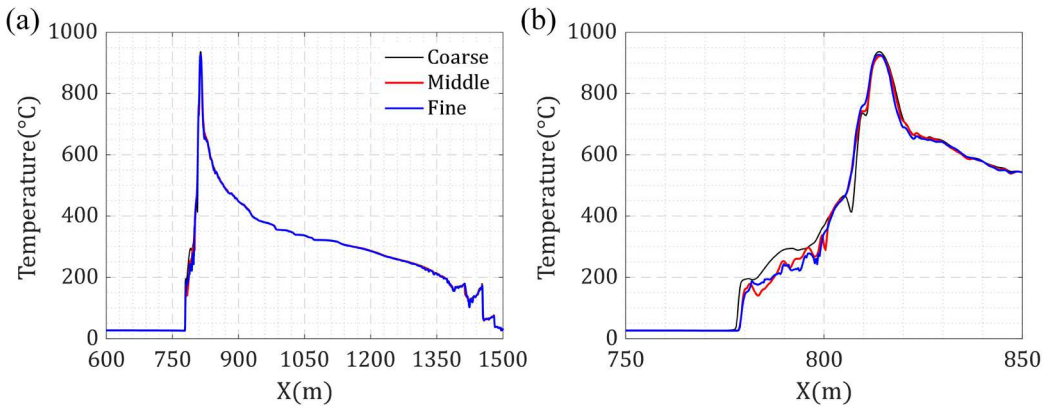

Fig. 8. Temperature curves along the length of the tunnel under 70kPa ambient pressure at 240 s.

4 Numerical results

4.1. Influence of the ambient pressure

This part mainly studies the influence of the change of ambient pressure on the fire transport characteristics in the tunnel under the action of the slipstream induced by the movement of the subway train. After the subway train stops in the tunnel after 30s, the location of the subway train is in $x = 680m(tail) - 820m(head)$, the location of the fire source is between 804-812, and the center of the fire is 808m. Fig 9 shows the longitudinal velocity distribution in the annular space between the subway train and the tunnel under different ambient pressures. It shows that with the decrease of pressure, the longitudinal velocity decreases, but according to [46], the smoke speed increases with the decrease of pressure for stationary fire , so the slipstream caused by train front sequence movement changes the law of longitudinal velocity in the annular space. When the train stops for 90s ($t = 120s$), the smoke under the 50kpa ambient pressure begins to flow back and spreads again through the head to the tail of the train. With the increase of atmospheric pressure, the time of smoke back-layer is delayed. Fig. 10 shows the velocity variation at the tunnel roof over time at $x = 808m, z = 4.75m$ for three different ambient pressure. According to the velocity curve of this point, the specific time when the smoke begins to flow back is inferred, that is, when the velocity is zero, representing the flowing back of the smoke. As is shown in Fig.10, the time for the smoke under 50kPa, 75kPa and 100kPa to spread to the tail of the car is 125s, 164s and 203s, respectively. Therefore, when a fire breaks out in a subway train at lower ambient atmospheric pressure, mechanical ventilation should be turned on earlier so that the smoke can always spread downstream.

The temperature change with time around the train in $y = 0$ section under different

ambient pressures is shown in Fig. 11-13. At $t=15s$, the train slows down for 5s, and the train speed is $15m/s$, the high temperature region and smoke are mainly concentrated at the bottom of the train. Due to the action of the longitudinal wind speed opposite to the direction of the train running in the annular space, it spreads to the rear (downstream). At $t=25s$ and $t=30s$, the longitudinal wind speed in the annular space weakens, and with the smoke spreading to the rear of the car, driven by thermal buoyancy, it spreads to the top of the tunnel, resulting in a wider range of high temperature area and smoke concentration distribution. Within the 90s after the train stops in the tunnel $(30s \le t \le 120s)$, the piston wind plays a decisive role in the smoke movement. From the temperature and smoke distribution, the smoke spreads upstream during this period. After that, the smoke flows back in turn, as the pressure increases from 50kpa to 100kpa. A comparative analysis of Fig. 11-13 shows that the temperature distribution, smoke concentration and the back-layer length increase with the decrease of ambient pressure. Under a certain HRR, lower ambient pressure leads to lower air density, less fresh air quality entering the smoke layer during smoke diffusion, and lower ambient pressure leads to lower smoke entrainment coefficient [46], these two factors will lead to higher smoke temperature and smoke concentration, and larger back-layer length. In addition, it can be observed from Fig. 11-13 that near the fire source, the driving buoyancy is large, resulting in serious smoke concentration fluctuations.

Fig. 14 shows the temperature variation along the length of the tunnel over time at $y=0, z=4.75m$ for three different ambient pressure at 30 s, 60 s, 120 s, 150s, 180s and 240 s. Due to the combined effect of blockage and piston wind, the temperature distribution of the tunnel is asymmetrical relative to the center of the fire source. It can be seen from the Fig. 14 that the maximum temperature under different pressure decreases firstly and increases gradually under the action of piston wind and thermal buoyancy which is consistent with the analysis in (N. Zhang et al., 2018a), and the position of the maximum is also changing. The difference between 50kpa and 75kpa is greater than that between 75kpa and 100kpa, indicating that the influence of ambient pressure on smoke diffusion decreases with the increase of pressure.

Table 2 presents a summary of the smoke front at different time under different ambient pressure. The smoke is found to move farther over time before the mechanical ventilation is turned on. The larger the ambient pressure is, the shorter the distance over which smoke travels becomes. The same pattern is observed at other moments, but there are some variations in the size of the difference.

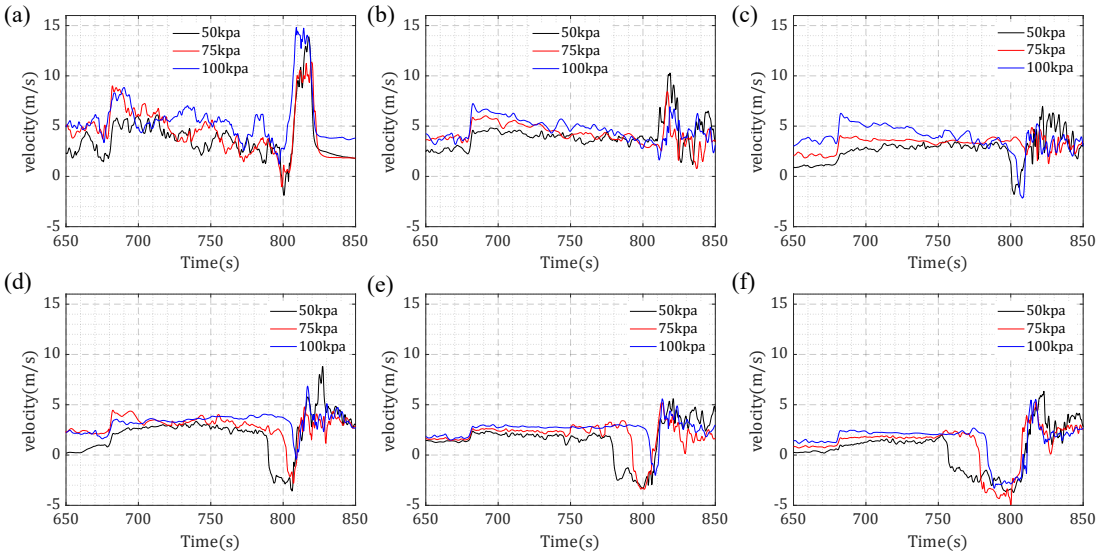

Fig. 9. Velocity curves along the length of the tunnel under different ambient pressure at (a) 30 s, (b) 60 s, (c) 120 s, (d) 150s, (e) 180s and (f) 240 s.

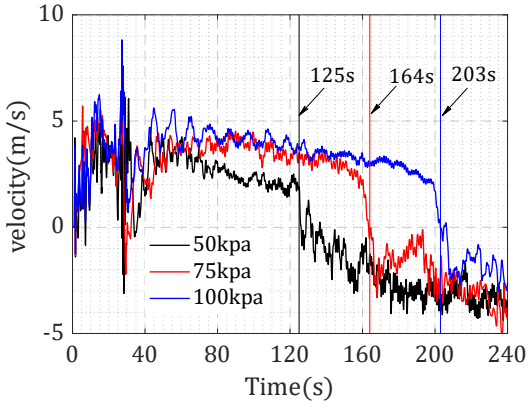

Fig. 10. Velocity variation over time at $x = 808m, z = 4.75m$ under different ambient pressure.

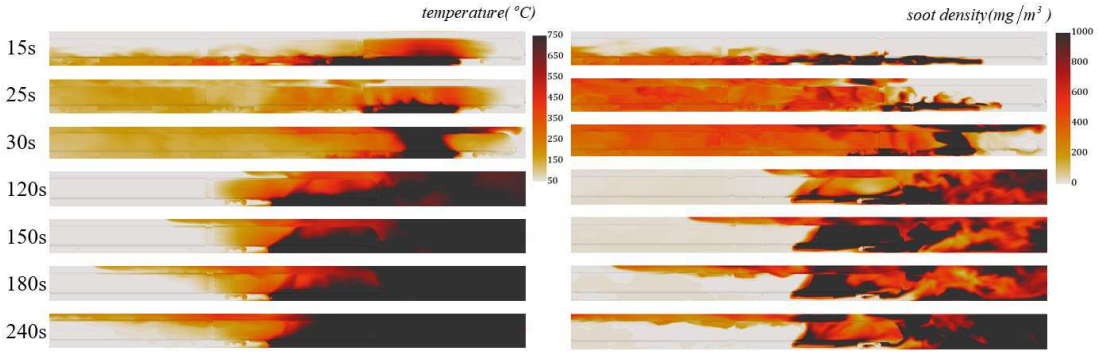

Fig. 11. Temperature and smoke around the train under 50kPa ambient pressure at different time

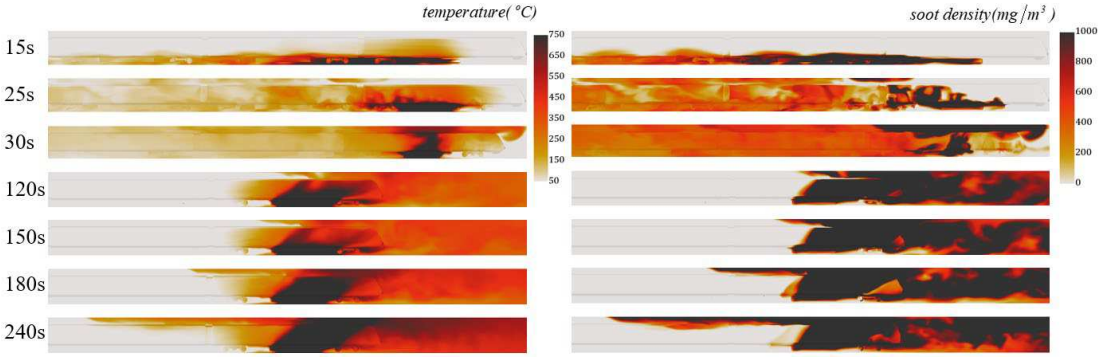

Fig. 12. Temperature and smoke around the train under 75kPa ambient pressure at different time

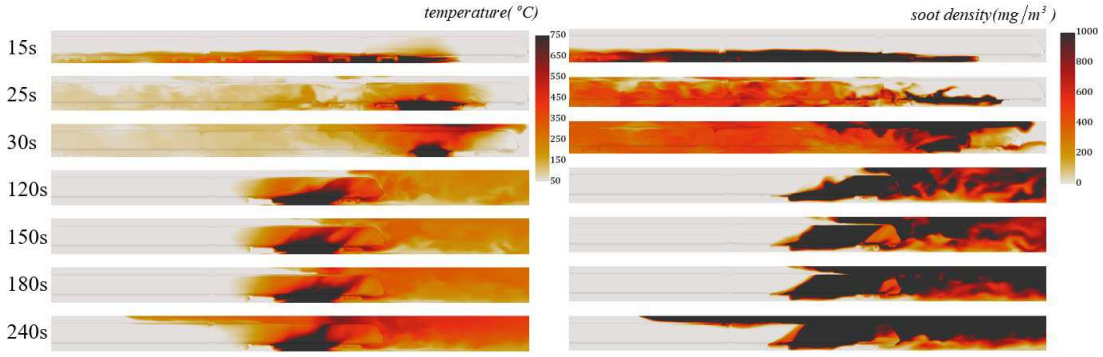

Fig. 13. Temperature and smoke around the train under 100kPa ambient pressure at different time

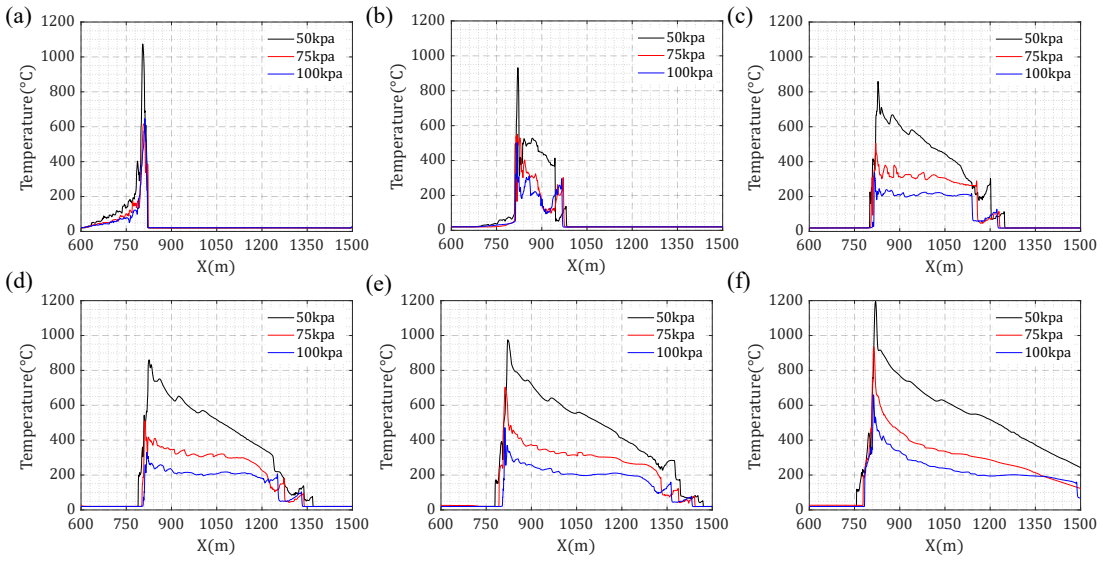

Fig. 14. Temperature curves along the length of the tunnel under different ambient pressure at (a) 30 s, (b) 60 s, (c) 120 s, (d) 150s, (e) 180s and (f) 240 s.

Table 2 Smoke front at different time under different ambient pressure (unit: m).

Pressure (*kpa*)	Time(s)								
	30	60	90	120	150	180	210	240	270
50	821	982	1126	1252	1375	1475	1500	1500	1500
75	822	976	1116	1238	1348	1450	1500	1500	1500

100	821	972	1111	1230	1335	1437	1500	1500	1500

4.2. Influence of tunnel inclination angle

The smoke movement and temperature distribution of static fire sources in horizontal and inclined tunnels have been widely studied. However, the smoke movement and temperature distribution under the combined effect of piston wind caused by train movement and the stack effect induced by inclined tunnel have not been seen yet. According to previous research, the induced longitudinal velocity induced by stack effect because of the tunnel inclination plays a leading role in distribution of temperature and smoke. So, this part mainly studies the influence of the change of tunnel inclination angle on the fire transport characteristics in the tunnel

The longitudinal velocity distribution with time around the train in $y=0$ section under different tunnel inclination angles is shown in Fig. 15-17. Taking Fig. 15 as an example, from 10s to 30s, the direction of the piston wind caused by train movement in the annular space changes from opposite direction to the same direction of train movement. Between 30s and 180s, although the train has stopped, the piston wind caused by the previous movement still exists, and under the action of the piston wind, the smoke moves downstream all the time, and due to the influence of thermal buoyancy near the fire source, the fluctuation of the smoke is consistent with that in Fig. 11, until the time is 240s (specific time is 205s in Fig.10), the smoke begins to flow back, and the wind speed in the upstream annular space becomes negative again. According to the previous study on the static fire source of inclined tunnel and comparative analysis of Fig. 15-17, the longitudinal velocity caused by stack effect is from the downstream to upstream when the tunnel inclination angle is negative (Fig. 16) which will counteract the piston wind caused by train movement and cause the smoke to return to the upstream in advance. When the tunnel inclination is positive, the situation is just the opposite. the longitudinal velocity caused by the stack effect is from upstream to downstream (Fig. 17), which strengthens the piston wind and the smoke never flows back towards the upstream within the simulation time of this paper. Fig. 18 shows the velocity variation at the tunnel roof over time at $x=808m, z=4.75m$ for three different tunnel inclination angles. As is shown in Fig.18, the time for the smoke under α=0°and-1.5° to spread to the upstream is 123s and 203s respectively, the smoke under +1.5° never flows back towards the upstream. Therefore, when a fire breaks out in a subway train at negative tunnel inclination angle, mechanical ventilation should be turned on earlier so that the smoke can always spread downstream.

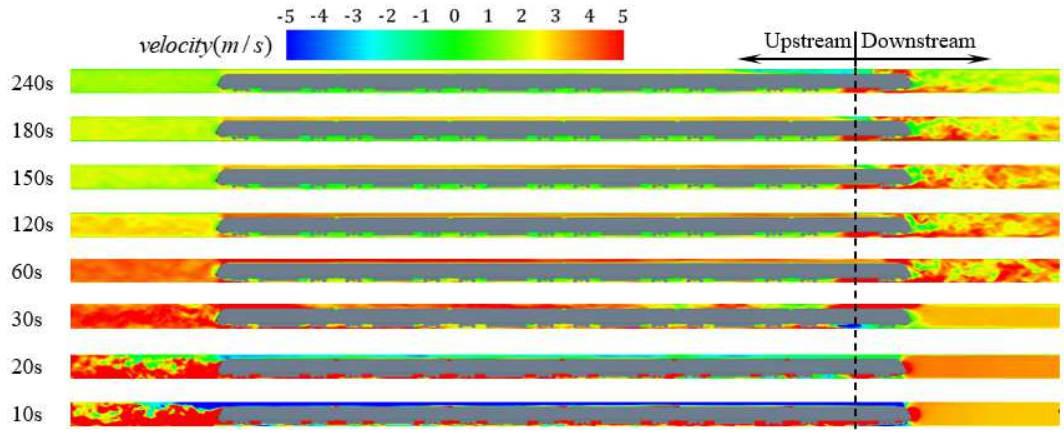

Fig. 15. Velocity distribution around the train under α=0° tunnel inclination angle at different time

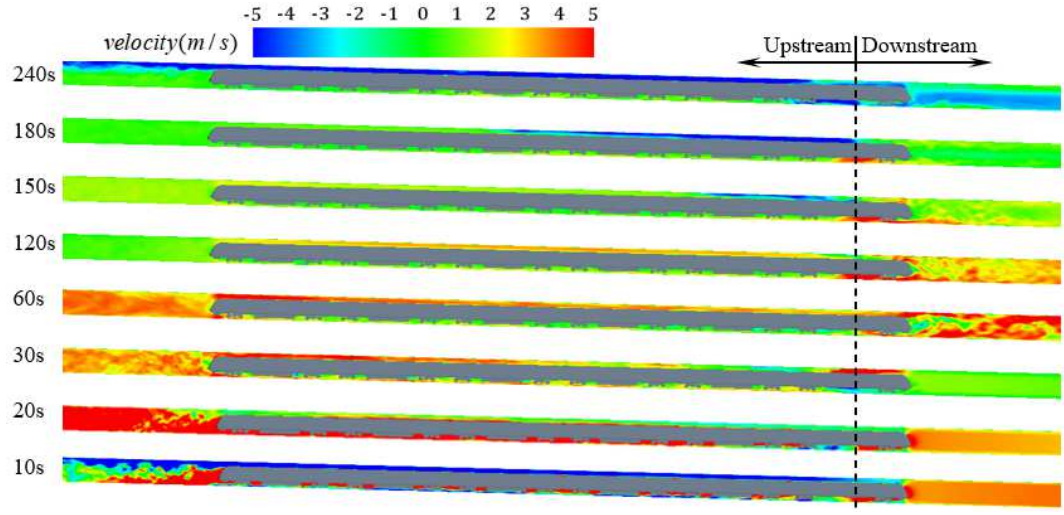

Fig. 16. Velocity distribution around the train under α=-1.5° tunnel inclination angle at different time

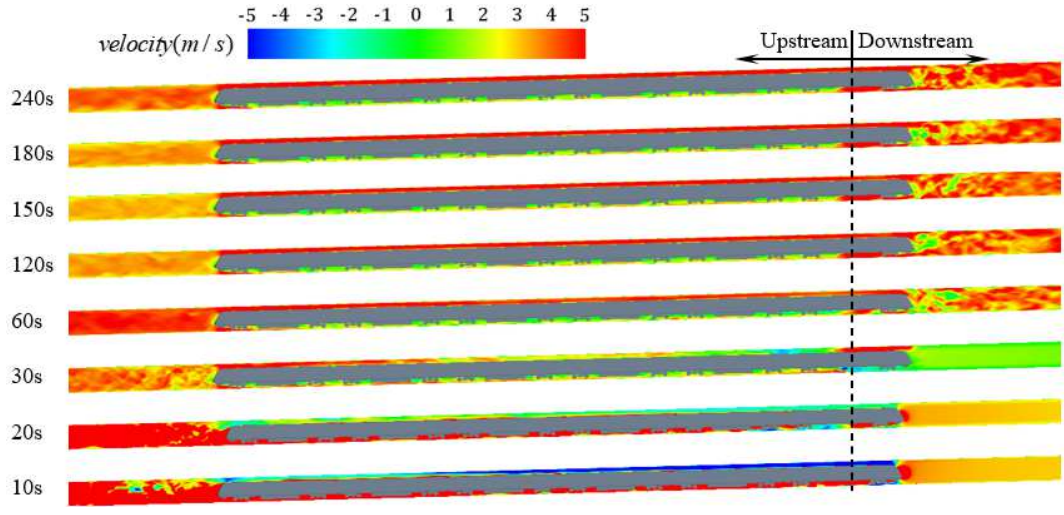

Fig. 17. Velocity distribution around the train under α=+1.5° tunnel inclination angle at different

time

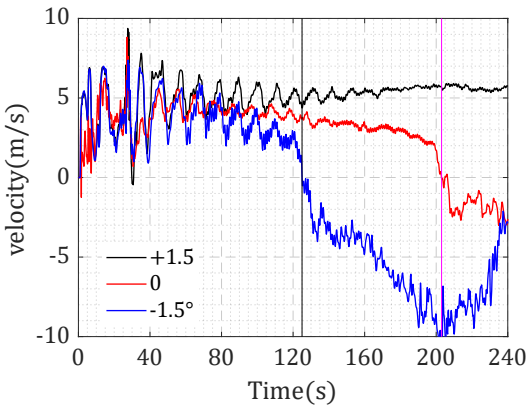

Fig. 18. Velocity variation over time at $x = 808m$ under different tunnel inclination angles.

Fig. 19 shows the temperature variation along the length of the tunnel over time at $y = 0, z = 4.75m$ for three different tunnel inclination angles at 30 s, 60 s, 120 s, 150s, 180s and 240 s. The trend of the overall temperature distribution is roughly the same for the three tunnel inclination angles at 30 s and 60 s, and it can also be seen from Fig. 15-17 that the longitudinal velocity distribution is basically the same, and the smoke distribution is mainly dominated by piston wind, and the longitudinal airflow induced by the stack effect needs a certain time to spread. After 90s, the longitudinal airflow induced by the stack effect plays a leading role, resulting in a wider distribution of high temperature and a larger maximum temperature for the negative inclination angle of the tunnel. In order to better understand the influence of the inclined angle of the tunnel on smoke transport, Fig. 20 and 21 show the distribution of temperature and smoke concentration around the train with time. Except that it can be seen intuitively that the positive inclination angle of the tunnel can effectively prevent the smoke countercurrent, the temperature and smoke concentration near the fire source are also lower, mainly due to the larger longitudinal velocity, which strengthens the mixing of smoke and fresh air and improves the entrainment effect efficiency.

Table 3 summarizes the specific positions of the smoke front upstream and downstream of the fire source at different tunnel inclination angles with time. It can be seen from the table that when the time is less than 90s, the upstream smoke front is basically the same, and there is only a difference in the downstream, which is the joint action of piston wind and thermal buoyancy. After 90s, from the above analysis, the longitudinal airflow induced by the stack effect affects the temperature and smoke distribution, resulting in the upstream smoke front of the negative tunnel inclination angle is far away from the fire source, and the downstream smoke front is

closer to the fire source.

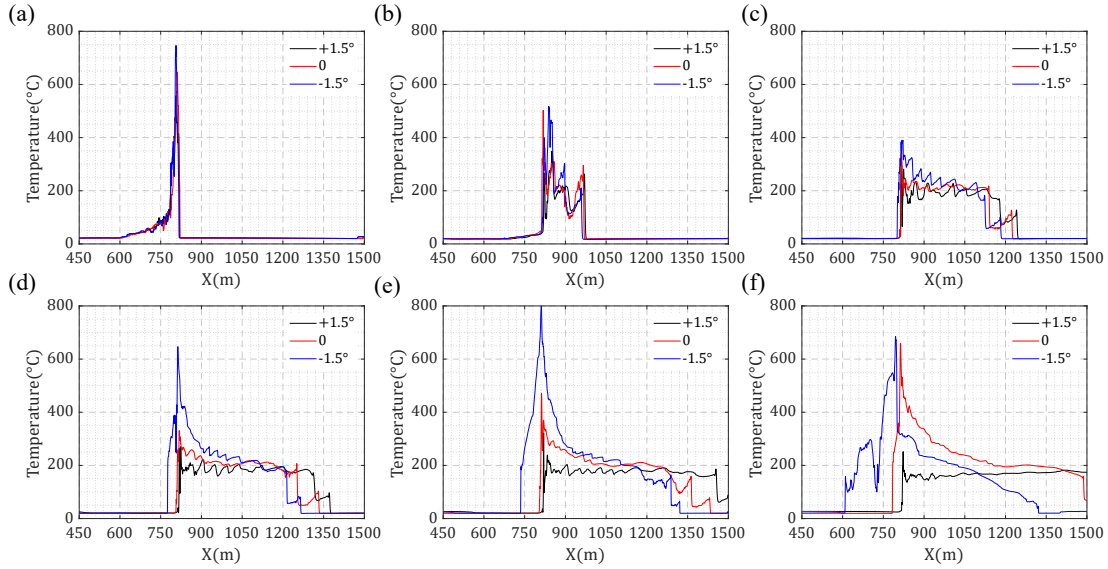

Fig. 19. Temperature curves along the length of the tunnel under different ambient pressure at (a) 30 s, (b) 60 s, (c) 120 s, (d) 150s, (e) 180s and (f) 240 s.

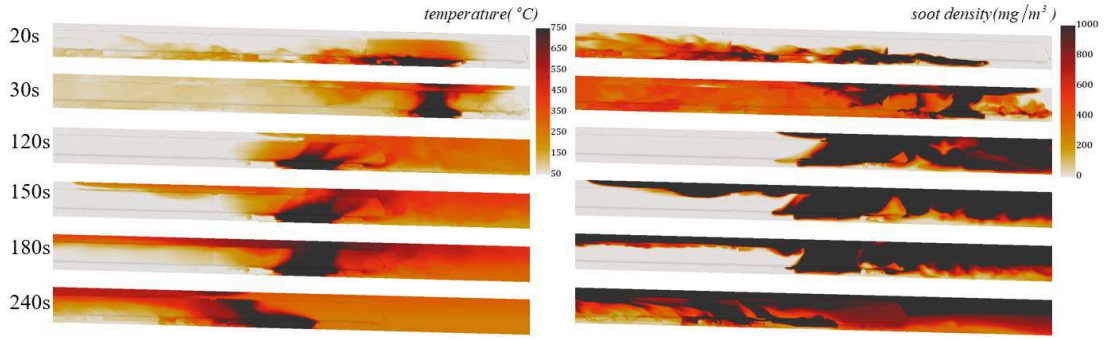

Fig. 20. Temperature and smoke around the train under α=-1.5° tunnel inclination angle at different time

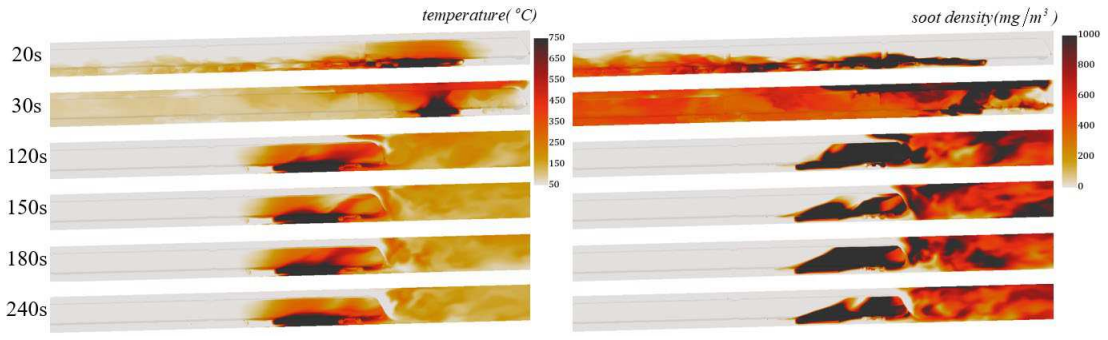

Fig. 21. Temperature and smoke around the train under α=+1.5° tunnel inclination angle at different time

Table 3 Smoke front at different time under different tunnel inclination (unit: m).

Inclination angle (◦)	Direction	Time(s)								
		30	60	90	120	150	180	210	240	270
+1.5°	upstream	600	684	801	815	811	812	811	812	810
	downstream	820	977	1123	1247	1376	1500	1500	1500	1500
0	upstream	600	685	804	812	807	803	794	782	768
	downstream	821	972	1111	1230	1335	1437	1500	1500	1500
-1.5°	upstream	600	683	800	802	774	735	678	608	538
	downstream	818	964	1089	1185	1268	1323	1340	1326	1268

5 Conclusions

The IDDES turbulence model based on $k\omega-sst$ RANS combined with the overset grid technology is used to simulate the subway train movement and the detailed flow field. The distribution characteristics of velocity field, temperature field and smoke concentration field are studied in detail. The effects of ambient pressure and tunnel inclination angle on the smoke transport of moving train in a subway tunnel were investigated in this paper. The results can be summarized as follows:

- For the certain HRR, the soot density of smoke and temperature increases with reduced ambient pressure, because the decrease of pressure leads to the decrease of air density, which leads to the weakening of air entrainment. The difference between 50kpa and 75kpa is greater than that between 75kpa and 100kpa, indicating that the influence of ambient pressure on smoke diffusion decreases with the increase of ambient pressure. When a fire breaks out in a subway train at lower ambient atmospheric pressure, the smoke flows back early due to the too low atmospheric pressure, so that mechanical ventilation should be turned on as early as possible so that the smoke can always spread downstream.
- The longitudinal velocity caused by stack effect is from the downstream to upstream when the tunnel inclination angle is negative which will counteract the piston wind caused by train movement and cause the smoke to return to the upstream in advance. When the tunnel inclination is positive, the longitudinal velocity caused by the stack effect is from upstream to downstream, which strengthens the piston wind.
- Within 90s, the temperature and soot density of smoke distribution is dominated by the piston wind, after 90s, the longitudinal airflow induced by the stack effect plays a leading role, resulting in a wider distribution of high temperature and a larger maximum temperature for the negative inclination angle of the tunnel.

As the fire source location and heat release rate are fixed in this paper, and no ventilation settings are adopted, it is hoped that the effects of fire source location, heat release rate and

ventilation on smoke transport in tunnels with different ambient pressures and inclined angles can be studied in the future.

Acknowledgements

The authors acknowledge the experimental and computational resources provided by the High-Speed Train Research Center of Central South University, China. This study is supported by the China Scholarship Council (File No. 201906370098) and Graduate Student Independent Innovation Project of Central South University (Grant No. 2020zzts117)

Reference

Bai, Y., Zeng, Y., Zhang, X., Yan, X., Ruan, L., Zhou, X., 2016. Numerical and experimental study on the flow field induced by a train urgently speeding to the rescue station. Tunn. Undergr. Sp. Technol. https://doi.org/10.1016/j.tust.2016.04.008

Cafaro, E., Bertola, V., 2014. Fires in Tunnels: Experiments and Modelling. Open Thermodyn. J. 4, 156–166. https://doi.org/10.2174/1874396x01004010156

Chaabat, F., Salizzoni, P., Creyssels, M., Mos, A., Wingrave, J., Correia, H., Marro, M., 2020. Smoke control in tunnel with a transverse ventilation system: An experimental study. Build. Environ. https://doi.org/10.1016/j.buildenv.2019.106480

Chen, G., Li, X.B., Liu, Z., Zhou, D., Wang, Z., Liang, X.F., Krajnovic, S., 2019. Dynamic analysis of the effect of nose length on train aerodynamic performance. J. Wind Eng. Ind. Aerodyn. https://doi.org/10.1016/j.jweia.2018.11.021

Chow, W.K., Dang, J.F., Gao, Y., Chow, C.L., 2017. Dependence of flame height of internal fire whirl in a vertical shaft on fuel burning rate in pool fire. Appl. Therm. Eng. https://doi.org/10.1016/j.applthermaleng.2017.04.108

Chow, W.K., He, Z., Gao, Y., 2011. Internal fire whirls in a vertical shaft. J. Fire Sci. https://doi.org/10.1177/0734904110378974

Cong, H.Y., Wang, X.S., Zhu, P., Jiang, T.H., Shi, X.J., 2017. Improvement in smoke extraction efficiency by natural ventilation through a board-coupled shaft during tunnel fires. Appl. Therm. Eng. https://doi.org/10.1016/j.applthermaleng.2017.02.092

Du, T., Yang, L., Yang, D., Dong, S., Ji, W., 2020. On the backlayering flow of the buoyant contaminants in a tunnel with forced longitudinal ventilation. Build. Environ. https://doi.org/10.1016/j.buildenv.2020.106798

Fan, C.G., Jin, Z.F., Zhang, J.Q., Zhu, H.Y., 2017. Effects of ambient wind on thermal smoke exhaust from a shaft in tunnels with natural ventilation. Appl. Therm. Eng. https://doi.org/10.1016/j.applthermaleng.2017.02.017

Gannouni, S., Maad, R. Ben, 2015. Numerical study of the effect of blockage on critical velocity and backlayering length in longitudinally ventilated tunnel fires. Tunn. Undergr. Sp. Technol. 48, 147–155. https://doi.org/10.1016/j.tust.2015.03.003

Hu, L.H., Chen, L.F., Wu, L., Li, Y.F., Zhang, J.Y., Meng, N., 2013a. An experimental investigation and correlation on buoyant gas temperature below ceiling in a slopping tunnel fire. Appl. Therm. Eng. https://doi.org/10.1016/j.applthermaleng.2012.07.043

Hu, L.H., Huo, R., Li, Y.Z., Wang, H.B., Chow, W.K., 2005. Full-scale burning tests on studying smoke temperature and velocity along a corridor. Tunn. Undergr. Sp. Technol. https://doi.org/10.1016/j.tust.2004.08.007

Hu, L.H., Tang, W., Chen, L.F., Yi, L., 2013b. A non-dimensional global correlation of maximum gas temperature beneath ceiling with different blockage-fire distance in a longitudinal ventilated tunnel. Appl. Therm. Eng. https://doi.org/10.1016/j.applthermaleng.2013.03.021

Ji, J., Bi, Y., Venkatasubbaiah, K., Li, K., 2016. Influence of aspect ratio of tunnel on smoke temperature distribution under ceiling in near field of fire source. Appl. Therm. Eng. https://doi.org/10.1016/j.applthermaleng.2016.06.086

Ji, J., Guo, F., Gao, Z., Zhu, J., Sun, J., 2017. Numerical investigation on the effect of ambient pressure

on smoke movement and temperature distribution in tunnel fires. Appl. Therm. Eng. https://doi.org/10.1016/j.applthermaleng.2017.03.026
Ji, J., Han, J.Y., Fan, C.G., Gao, Z.H., Sun, J.H., 2013. Influence of cross-sectional area and aspect ratio of shaft on natural ventilation in urban road tunnel. Int. J. Heat Mass Transf. https://doi.org/10.1016/j.ijheatmasstransfer.2013.08.033
Ji, J., Wang, Z., Ding, L., Yu, L., Gao, Z., Wan, H., 2019. Effects of ambient pressure on smoke movement and temperature distribution in inclined tunnel fires. Int. J. Therm. Sci. https://doi.org/10.1016/j.ijthermalsci.2019.106006
Jiang, X., Liao, X., Chen, S., Wang, J., Zhang, S., 2018. An experimental study on plug-holing in tunnel fire with central smoke extraction. Appl. Therm. Eng. https://doi.org/10.1016/j.applthermaleng.2018.04.052
Ko, Y.J., Hadjisophocleous, G. V., 2013. Study of smoke backlayering during suppression in tunnels. Fire Saf. J. https://doi.org/10.1016/j.firesaf.2013.03.001
Lee, S.R., Ryou, H.S., 2006. A numerical study on smoke movement in longitudinal ventilation tunnel fires for different aspect ratio. Build. Environ. https://doi.org/10.1016/j.buildenv.2005.03.010
Lemaire, T., Kenyon, Y., 2006. Large scale fire tests in the Second Benelux Tunnel. Fire Technol. 42, 329–350. https://doi.org/10.1007/s10694-006-8434-4
Li, X.B., Chen, G., Wang, Z., Xiong, X.H., Liang, X.F., Yin, J., 2019. Dynamic analysis of the flow fields around single- and double-unit trains. J. Wind Eng. Ind. Aerodyn. https://doi.org/10.1016/j.jweia.2019.02.015
Li, Y.Z., Lei, B., Ingason, H., 2011. The maximum temperature of buoyancy-driven smoke flow beneath the ceiling in tunnel fires. Fire Saf. J. https://doi.org/10.1016/j.firesaf.2011.02.002
Liang, X., Chen, G., Li, X., Zhou, D., 2020. Numerical simulation of pressure transients caused by high-speed train passage through a railway station. Build. Environ. 107228. https://doi.org/10.1016/j.buildenv.2020.107228
Liu, C., Li, L., 2020. How do subways affect urban passenger transport modes?—Evidence from China. Econ. Transp. 23. https://doi.org/10.1016/j.ecotra.2020.100181
Mei, F., Tang, F., Ling, X., Yu, J., 2017. Evolution characteristics of fire smoke layer thickness in a mechanical ventilation tunnel with multiple point extraction. Appl. Therm. Eng. https://doi.org/10.1016/j.applthermaleng.2016.09.064
Meng, N., Liu, X., Li, X., Liu, B., 2018. Effect of blockage ratio on backlayering length of thermal smoke flow in a longitudinally ventilated tunnel. Appl. Therm. Eng. https://doi.org/10.1016/j.applthermaleng.2017.12.064
Meng, N., Wang, Q., Liu, Z., Li, X., Yang, H., 2017. Smoke flow temperature beneath tunnel ceiling for train fire at subway station: Reduced-scale experiments and correlations. Appl. Therm. Eng. https://doi.org/10.1016/j.applthermaleng.2017.01.027
Migoya, E., García, J., Crespo, A., Gago, C., Rubio, A., 2011. Determination of the heat release rate inside operational road tunnels by comparison with CFD calculations. Tunn. Undergr. Sp. Technol. https://doi.org/10.1016/j.tust.2010.05.001
Oka, Y., Atkinson, G.T., 1995. Control of smoke flow in tunnel fires. Fire Saf. J. https://doi.org/10.1016/0379-7112(96)00007-0
Overview, P., Guide, U., n.d. Simcenter STAR-CCM + Product Overview.
Tang, F., Cao, Z.L., Chen, Q., Meng, N., Wang, Q., Fan, C.G., 2017. Effect of blockage-heat source distance on maximum temperature of buoyancy-induced smoke flow beneath ceiling in a longitudinal ventilated tunnel. Int. J. Heat Mass Transf. https://doi.org/10.1016/j.ijheatmasstransfer.2017.02.021
Tang, F., Li, L.J., Mei, F.Z., Dong, M.S., 2016. Thermal smoke back-layering flow length with ceiling extraction at upstream side of fire source in a longitudinal ventilated tunnel. Appl. Therm. Eng. https://doi.org/10.1016/j.applthermaleng.2016.05.173
Tian, X., Zhong, M., Shi, C., Zhang, P., Liu, C., 2017. Full-scale tunnel fire experimental study of fire-induced smoke temperature profiles with methanol-gasoline blends. Appl. Therm. Eng. https://doi.org/10.1016/j.applthermaleng.2017.01.099
Vauquelin, O., Mégret, O., 2002. Smoke extraction experiments in case of fire in a tunnel. Fire Saf. J. https://doi.org/10.1016/S0379-7112(02)00014-0
Vauquelin, O., Telle, D., 2005. Definition and experimental evaluation of the smoke “confinement velocity” in tunnel fires. Fire Saf. J. https://doi.org/10.1016/j.firesaf.2005.02.004
Wang, Y.F., Jiang, J., Zhu, D., 2009. Full-scale experiment research and theoretical study for fires in tunnels with roof openings. Fire Saf. J. https://doi.org/10.1016/j.firesaf.2008.08.001

Wang, Y.F., Sun, X.F., Liu, S., Yan, P.N., Qin, T., Zhang, B., 2016. Simulation of back-layering length in tunnel fire with vertical shafts. Appl. Therm. Eng. https://doi.org/10.1016/j.applthermaleng.2016.08.081

Wang, Z., Zhou, D., Krajnovic, S., Liu, H., 2020. Moving model test of the smoke movement characteristics of an on-fire subway train running through a tunnel. Tunn. Undergr. Sp. Technol. 96. https://doi.org/10.1016/j.tust.2019.103211

Weng, M.C., Lu, X.L., Liu, F., Du, C.X., 2016. Study on the critical velocity in a sloping tunnel fire under longitudinal ventilation. Appl. Therm. Eng. https://doi.org/10.1016/j.applthermaleng.2015.10.059

Weng, M.C., Yu, L.X., Liu, F., Nielsen, P. V., 2014. Full-scale experiment and CFD simulation on smoke movement and smoke control in a metro tunnel with one opening portal. Tunn. Undergr. Sp. Technol. https://doi.org/10.1016/j.tust.2014.02.007

Yan, T., MingHeng, S., YanFeng, G., JiaPeng, H., 2009. Full-scale experimental study on smoke flow in natural ventilation road tunnel fires with shafts. Tunn. Undergr. Sp. Technol. https://doi.org/10.1016/j.tust.2009.06.001

Yao, H.W., Meng, D., Zheng, Y.P., Liang, D., 2016. Analysis on causes of subway fire alarm linkage strategy, in: Proceedings - 2016 International Conference on Robots and Intelligent System, ICRIS 2016. https://doi.org/10.1109/ICRIS.2016.22

Yao, Y., Cheng, X., Zhang, S., Zhu, K., Shi, L., Zhang, H., 2016. Smoke back-layering flow length in longitudinal ventilated tunnel fires with vertical shaft in the upstream. Appl. Therm. Eng. https://doi.org/10.1016/j.applthermaleng.2016.07.027

Zhang, N., Lu, Z., Zhou, D., 2018a. Influence of train speed and blockage ratio on the smoke characteristics in a subway tunnel. Tunn. Undergr. Sp. Technol. https://doi.org/10.1016/j.tust.2018.01.010

Zhang, N., Lu, Z., Zhou, D., 2018b. Influence of train speed and blockage ratio on the smoke characteristics in a subway tunnel. Tunn. Undergr. Sp. Technol. 74, 33–40. https://doi.org/10.1016/j.tust.2018.01.010

Zhang, S., Cheng, X., Yao, Y., Zhu, K., Li, K., Lu, S., Zhang, R., Zhang, H., 2016. An experimental investigation on blockage effect of metro train on the smoke back-layering in subway tunnel fires. Appl. Therm. Eng. https://doi.org/10.1016/j.applthermaleng.2015.12.085

Zhang, S., Cheng, X., Zhu, K., Yao, Y., Shi, L., Zhang, H., 2017. Experimental study on curved flame characteristics under longitudinal ventilation in a subway tunnel. Appl. Therm. Eng. https://doi.org/10.1016/j.applthermaleng.2016.12.023

Zhang, X., Ma, J., Li, A., Lv, W., Zhang, W., Li, D., 2019. Ventilation for subway stations with adjustable platform doors created by train-induced unsteady airflow. Build. Environ. https://doi.org/10.1016/j.buildenv.2019.02.001

Zhang, Z., Zhang, H., Tan, Y., Yang, H., 2018. Natural wind utilization in the vertical shaft of a super-long highway tunnel and its energy saving effect. Build. Environ. https://doi.org/10.1016/j.buildenv.2018.08.062

Zhong, W., Tu, R., Yang, J.P., Liang, T.S., 2015. A study of the fire smoke propagation in subway station under the effect of piston wind. J. Civ. Eng. Manag. https://doi.org/10.3846/13923730.2014.890661

Zhou, D., Tian, H. qi, Zheng, J. li, Yan, X., 2015. Smoke movement in a tunnel of a running metro train on fire. J. Cent. South Univ. https://doi.org/10.1007/s11771-015-2511-0

Zhou, Y., Bi, H., Wang, H., Lei, B., 2020. Fire characteristics of rescue station inside railway tunnel with semi-transverse ventilation. Tunn. Undergr. Sp. Technol. https://doi.org/10.1016/j.tust.2020.103303